MATERIALS RESEARCH SOCIETY
SYMPOSIUM PROCEEDINGS VOLUME 571

Semiconductor Quantum Dots

Symposium held April 5–8, 1999, San Francisco, California, U.S.A.

EDITORS:

Steven C. Moss
The Aerospace Corporation
Los Angeles, California, U.S.A.

Daryush Ila
Alabama A&M University
Normal, Alabama, U.S.A.

Howard W.H. Lee
Lawrence Livermore National Laboratory
Livermore, California, U.S.A.

David J. Norris
NEC Research Institute
Princeton, New Jersey, U.S.A.

ORGANIZERS:

A. Paul Alivisatos
University of California, Berkeley
Berkeley, California, U.S.A.

Anupam Madhukar
University of Southern California
Los Angeles, California, U.S.A.

MRS
Materials Research Society
Warrendale, Pennsylvania

OPTICAL SPECTROSCOPY OF SINGLE SELF ASSEMBLED QUANTUM DOTS

E. DEKEL*, D. GERSHONI*, E. EHRENFREUND*, J.M. GARCIA** AND P.M. PETROFF**
*Physics Department and Solid State Institute, Technion-Israel Institute of Technology, Haifa 32000, Israel, dg@physics.technion.ac.il
**Materials Department, University of California, Santa Barbara, California 93106, USA

ABSTRACT

We applied low temperature diffraction limited confocal optical microscopy to spatially resolve, and spectroscopically study photoluminescence from single self-assembled semiconductor quantum dots. Using selective wavelength imaging we unambiguously demonstrated that a single photoexcited quantum dot emits light in a few very narrow spectral lines. By solving numerically a many body Hamiltonian for a model quantum dot, we show that the multi-line emission spectrum is due to optical transitions between confined exciton multiplexes. We explain the measured spectrum and its dependence on the power of either cw or pulsed excitation by analytically solving the coupled rate equations for the excitation relaxation between these exciton multiplexes.

INTRODUCTION

The study of electronic properties of semiconductor heterostructures of reduced dimensionality has been a subject of many recent extensive efforts. These efforts are motivated both by their potential device applications as well as by being an excellent stage for experimental studies of basic quantum mechanical principles. Semiconductor quantum dots (QDs) of nanometer size are of particular interest since carriers are confined there within dimensions smaller than their de-Broglie wavelength [1].

One of the simplest and therefore most common ways of producing semiconductor QDs is the Stranski and Krastanov (SK) self-assembled growth of strained QDs (SAQDs) [2,3,4]. In this growth mode, the elastic energy associated with the lattice mismatch strain between different epitaxially deposited semiconductor layers is minimized through the formation of small islands connected by a thin wetting layer [5]. These high crystalline quality islands are typically of pyramidal shape of 100-300 Å base dimensions and 20-80 Å height [6]. By capping these self assembled islands with an epitaxial layer of wider bandgap material and lattice constant which is similar to that of the substrate, high quality QDs are produced.

The presence of few confined carriers in such a small volume gives rise to correlated few carrier multiplexes [7-9] that are unstable otherwise. Therefore, the analysis of the optical studies of these systems is fundamentally different than the analysis of recombination processes in systems of higher dimensionality.

One of the main disadvantages of the SK growth mode is the size distribution of the SAQDs, typically about ±10% [6]. This size distribution, along with possible distributions in composition, strain and structural shape, give rise to a large non-uniformity of the SAQD's properties in general and inhomogeneous broadening of the optical spectral features in particular [1,3-6,10]. We overcome this obstacle by optically studying a single quantum dot.[11-14] We present continuous wave (cw) and pulsed photoluminescence (PL) measurements of the recombination processes in single SAQDs. For the analysis of the data we outline a theoretical model which quite systematically explains the measured PL spectra and quantitatively accounts for their dependence on the excitation power in both cw and pulsed mode.

Mat. Res. Soc. Symp. Proc. Vol. 571 © 2000 Mater

THEORETICAL MODEL

We describe the many-body Hamiltonian of a single QD in terms of its single carrier energies and wave functions,

$$H = H^{e}_{free} + H^{h}_{free} + H^{e-e}_{coul} + H^{e-h}_{coul} + H^{h-h}_{coul}, \quad (1)$$

where,

$$H^{h}_{free} = \sum_{j} \varepsilon_j b^{+}_j b_j \,, \; H^{e}_{free} = \sum_{i} \varepsilon_i a^{+}_i a_i \,, \quad (2)$$

$$H^{e-e}_{coul} = \frac{1}{2} \sum_{i_1,i_2,i_3,i_4} a^{+}_{i_1} a^{+}_{i_2} a_{i_3} a_{i_4} G_{i_1,i_2,i_3,i_4} \,, \quad (3)$$

$$H^{e-h}_{coul} = - \sum_{i_1,j_2,j_3,i_4} a^{+}_{i_1} a_{i_4} b^{+}_{j_3} b_{j_2} G_{i_1,j_2,j_3,i_4} + \sum_{j_1,i_2,j_3,i_4} a^{+}_{i_2} a_{i_4} b^{+}_{j_3} b_{j_1} G_{j_1,i_2,j_3,i_4} \quad (4)$$

$$H^{h-h}_{coul} = \frac{1}{2} \sum_{j_1,j_2,j_3,j_4} b^{+}_{j_1} b^{+}_{j_2} b_{j_3} b_{j_4} G_{j_1,j_2,j_3,j_4} \,. \quad (5)$$

In Eqs. (2)-(5), a_i, b_j (a^{+}_i, b^{+}_j) are the annihilation (creation) operators for electrons and holes, respectively, and ε_i, ε_j are their corresponding one particle energy levels within the QD. The summation index i (j) runs over all the electron (hole) one particle states (spin-degenerate states are included). The Coulomb interaction terms, Eqs. (3)-(5), can be expressed in terms of the one particle (electron and hole) envelope wavefunctions $\phi_{l,B}(\bar{x})$ as follows,

$$G_{l_1,l_2,l_3,l_4} = \delta_{S_4,S_1}\delta_{S_3,S_2} \iint d^3x d^3x' \phi^{*}_{l_1,B}(\bar{x}) \phi^{*}_{l_2,B}(\bar{x}') \frac{e^2}{\varepsilon|\bar{x}-\bar{x}'|} \phi_{l_3,B}(\bar{x}') \phi_{l_4,B}(\bar{x}) \,, \quad (6)$$

where δ_{ij} is the Kronecker delta and s_i and e are the spin and charge of the respective single carrier state, B=C,V is the band index and l_i represents the set of quantum numbers that characterizes the single carrier envelope function.

We use a one-band model for both electrons and holes with envelope functions which are the analytical solutions of a potential structure described by a rectangular box of dimensions L_x, L_y, L_z, and infinite potential barriers,

$$\phi_{l,B}(\bar{x}) = \phi_{nx,ny,nz,B}(\bar{x}) = \sqrt{\frac{2^3}{L_x L_y L_z}} \sin\left(\frac{n_x \pi}{L_x} x\right) \sin\left(\frac{n_y \pi}{L_y} y\right) \sin\left(\frac{n_z \pi}{L_z} z\right) \,, \quad (7)$$

where n_x, n_y, n_z (=1,2,3...), are the quantum numbers associated with the respective axes. In our simple model, the small e-h exchange interaction[15], strictly vanishes. We numerically diagonalize the Hamiltonian (1) to yield all the multi-carrier energy levels and their corresponding wavefunctions. We study in this work an undoped sample in which carriers are excited optically. Therefore, we deal here only with neutral multi-carrier states with equal number of electrons and holes.

As an example, we describe in Fig. 1a few simple situations. First, we consider the case in which only one electron-hole pair (an "exciton") occupies the QD (Fig. 1a). If the Coulomb interaction within the pair can be ignored, it is readily seen that there are many possible different energy levels. Each one is four times degenerate due to the various electron and hole spin states (left side of Fig. 1a, where for simplicity only four levels are shown). We denote the four lowest energy states of the non-interacting pair by, $1e^{1}\uparrow 1h^{1}\uparrow$, $1e^{1}\uparrow 1h^{1}\downarrow$, $1e^{1}\downarrow 1h^{1}\uparrow$ and $1e^{1}\downarrow 1h^{1}\downarrow$,

respectively. Here $1e(h)^{1}$ means one electron (hole) in its lowest single carrier level (111). Similarly, assuming that the effective mass of the hole is larger than that of the electron, the degenerate states of the second energy level are denoted by $1e^{1}\uparrow 1h^{2}\uparrow$, $1e^{1}\uparrow 1h^{2}\downarrow$, $1e^{1}\downarrow 1h^{2}\uparrow$ and $1e^{1}\downarrow 1h^{2}\downarrow$, respectively. The situation in which two electrons and two holes (a "biexciton") occupy the dot can be similarly described. Here, there are many more possible states in a larger number of energy levels and, unlike the exciton case, the degeneracy is energy level dependent (Fig.1b, where for simplicity only 9 levels are shown). There are non-degenerate levels such as the lowest biexcitonic energy level $1e^{1}\uparrow 1e^{1}\downarrow 1h^{1}\uparrow 1h^{1}\downarrow$, in which all the participating single carrier electron and hole levels are full. There are also levels of 16 fold degeneracy like $1e^{1}1e^{2}1h^{1}1h^{2}$ in which 2 different electron and hole levels are half full. These levels are illustrated on the left side of Fig. 1b.

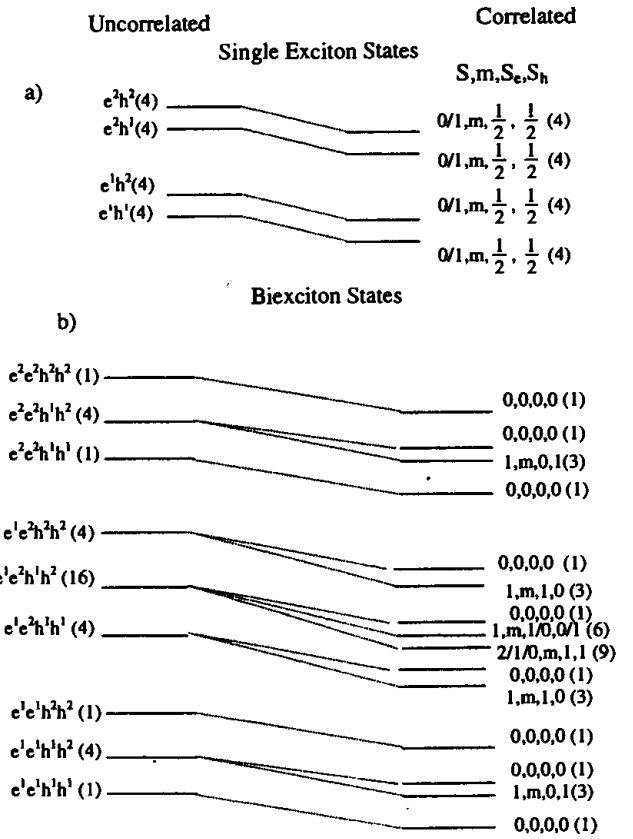

Fig. 1: Schematic description of the energy levels of the QD confined single- and bi-exciton multiplexes. On the left (right) side of the figure the levels are described without (with) the Coulomb interaction. The numbers in parentheses represent the level degeneracy and the symbols e^{i} (h^{j}) stand for electron (hole) in their i^{th} (j^{th}) single carrier level.

Since the Hamiltonian is spin independent, it commutes with spin operators. Therefore, their eigenvalues can be used to characterize the eigenstates of the full Hamiltonian (1). The "good" quantum numbers that we introduce [16] are the total electron (hole) spin $S^2_{e(h)}$, the total spin S^2, and its projection along the z-axis, S_z. In the single exciton case, as can be seen in the right side of Fig. 1, the Coulomb attraction gives rise to a rigid downward shift of all the energy levels. However, there is no degeneracy removal and all the excitonic levels remain four times degenerate.

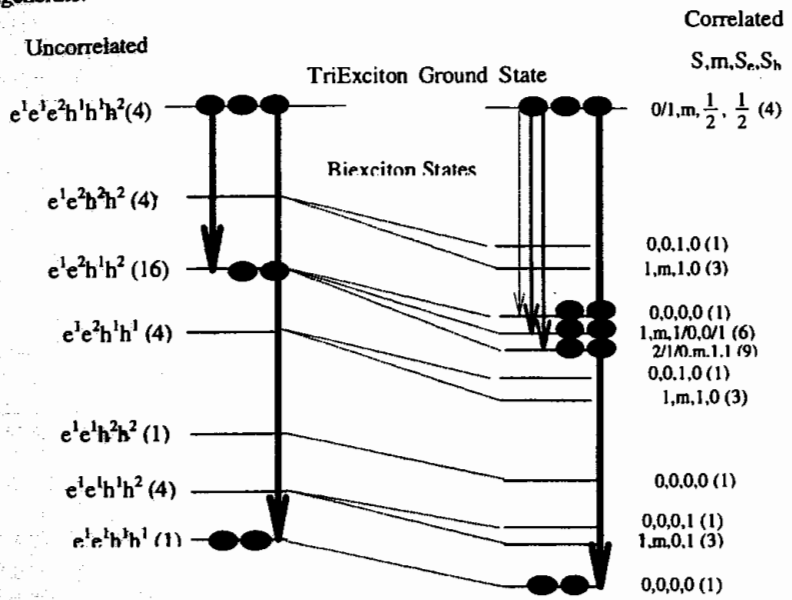

Fig 2: Schematic description of the allowed optical transitions between the ground tri-exciton energy level to the biexciton states, without (left side) and with (right side) the Coulomb interaction. The light (dark) gray vertical lines represent e^1h^1 (e^2h^2) pair recombination.

The situation is vastly different for the biexciton case. A noteworthy example is the 16 fold degenerate $1e^11e^21h^11h^2$ level. Here, the electron-electron (e-e) and hole-hole (h-h) exchange interactions partly remove the degeneracy by splitting it into three levels. The lowest level with $S^2_e=1$ $S^2_h=1$ is 9-fold degenerate. The second level with $S^2_e=1(0)$ $S^2_h=0(1)$ is six fold degenerate and a third, non-degenerate level exist, with $S^2_e=0$ and $S^2_h=0$.

There are several hundred degenerate energy levels for each N^{th} (N>2) exciton multiplex. Therefore, there are typically hundreds of allowed optical transitions of different photon energies between the $(N+1)^{th}$ to the N^{th} multiexciton cases. If the radiative rate is much slower than the thermalization rate, fast thermalization to the ground multiexcitonic states will significantly lower the number of these transitions. Our experimental observations [17] are definitely in agreement with this assumption. Therefore, only optical transitions from the ground energy level of each $(N+1)^{th}$ multiexciton to all possible levels of the N^{th} multiexciton are considered.

For illustration, we schematically display in Fig. 2 all the allowed optical transitions that result from the radiative annihilation of a tri-exciton in its ground energy level. The subsequent creation of a biexcitonic state is also described in the figure. In the non-correlated energy level

scheme (left side of Fig.2) only two optical transitions are allowed. The first is due to the recombination of an electron and a hole in their first one-carrier energy levels, and the second is due to the recombination of an electron and a hole in their second energy level. In the correlated carrier picture, however, (right side, Fig. 2) the first optical transition splits into two strong and one weak distinct transitions due to the splitting of the 16 times degenerate $e^1e^2h^1h^2$ energy level as discussed above. This behavior is not limited to this optical transition only. As can be readily understood, similar splitting occurs also in optical transitions between higher multiplexes of excitons. The e-e and h-h exchange-interactions are responsible for the line splitting described in Fig. 2. In addition, they give rise to a spectral red shift of optical transitions from successively higher multiplexes of multiexcitons, as demonstrated in Fig. 3. The red shift is caused by the number of exchange interactions, which increases with the number of carriers. Therefore, the sum of exchange interaction energies lowers the energy of the N+1 multiexciton levels more than it lowers the energy of the N multiexciton levels, thus causing successive red shift in the transition energies.

In Fig. 3 we present the calculated optical transitions due to the recombination of electrons and holes from the two lowest lying single carrier energy levels, as a function of the number of excitons within it. For these calculations a bandgap of 0.625 eV, dielectric constant of 15.0 and electron and hole effective masses of 0.023 and 0.6 electron rest mass, respectively, were used [18]. The QD dimensions L_x, L_y and L_z were set to 30.5, 30.0, and 5.0 nm, respectively, to best fit the experimental data (see below).

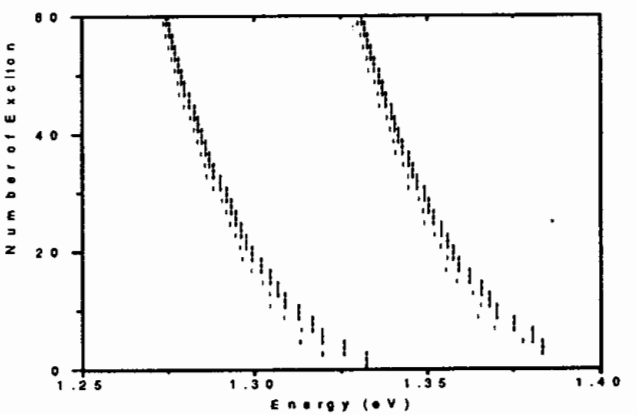

Fig 3: Vertical bars represent the calculated allowed optical transition energies of increasingly higher QD exciton multiplexes. By light gray vertical bars we denote optical transitions into the upper non-degenerate exchange-split states, which due to the lack of degeneracy have smaller intensity.

The figure demonstrates the following points: (a) At most six optical transitions are allowed for radiative recombination of an odd multiexciton ground state. (b) Only two transitions are allowed for recombination of an even multiexciton. (c) The same optical transition can be due to the recombination of up to 5 different exciton multiplexes. (d) The magnitude of the energy splitting and the spectral red shift for successively higher order multiexcitons rapidly decrease

with the number of excitons, causing the reduction of the transition energy to converge to a finite value. This value can be easily associated with the renormalized bandgap of a highly excited bulk semiconductor. We note here, that Fig. 3 describes the case of infinite potential barriers with an infinite number of discrete confined single carrier energy levels. In reality, however, we expect only a very few confined single electron levels before the onset of a spectral continuum. Therefore, the figure can only serve for a qualitative discussion of the experimental measurements. If we assume that all the non-radiative recombination rates are slower than the radiative ones (see below), then the multiexciton lifetimes can be directly determined from the calculated optical transitions. The lifetime of each N-excitonic multiplex is inversely proportional to the sum over all the allowed optical transitions from the ground level of this multiplex to the levels of the N-1 multiexciton.

At any given time only one, well defined, excitonic multiplex may exist in the QD. We define by n_i ($0< n_i <1$) the probability to find the i^{th}-excitonic multiplex in the QD. Thus, for example, n_0 is the probability to find the QD empty, and n_2 is the probability to find a biexciton in the QD. We describe the temporal evolution of an exciton multiplex by the following rate equation:

$$\frac{dn_i}{dt} = g_i - \frac{n_i}{\tau_i} + \frac{n_{i+1}}{\tau_{i+1}} - g_{i+1} \tag{8}$$

Here τ_i is the radiative lifetime of the ith-multiexciton and g_i is its photogeneration rate ($\tau_0=\infty$ and $g_0=0$). We note that in addition to the 'conventional' first three terms in Eq. (8) there is also a fourth term which describes the decrease in the i^{th}-multiexciton occupation probability due to the photogeneration of the $(i+1)^{th}$ multiexciton which causes the i^{th}-multiexciton to 'vanish'. The photogeneration rate of the i^{th}-multiexciton g_i can be expressed as, $g_i = n_{i-1}G$, where G is the total QD exciton photogeneration rate, which corresponds to the power of the external excitation source at a given time. As a consistency check, it is easy to show by direct differentiation of Eq. (8) that the sum of all the rate equations (8) vanishes.

When the QD is photoexcited by a continuous wave (cw) light source, G is a constant, and the QD will reach a steady state in which $dn_i/dt=0$ for all i. By substituting this into Eq. (8) we get a set of linear equations which we solve analytically to yield $n_i(G)$ ($i>0$),

$$n_i = n_0 G^i \prod_{j=1}^{i} \tau_j \quad , \quad n_0 = \frac{1}{1 + \tau_1 G + \tau_1\tau_2 G^2 + \ldots + G^N \prod_{j=1}^{N} \tau_j} \tag{9}$$

where N is the highest order multiexciton with non-vanishing occupation probability to be considered.

We now use the calculated optical transitions from each exciton multiplex (as given by Fig 3) to calculate the PL spectrum dependence on the excitation power. In Fig. 4 we present the calculated emission strength of a few spectral lines as a function of the excitation rate G. The figure demonstrates that the various spectral lines reach maximum at a comparable emission intensity, and that the spectrum shifts to the red as the excitation rate increases.

When the QD is photoexcited by a temporally short laser pulse, a well-defined exciton multiplex is generated in the QD within a short time after the pulse. The photogeneration rate is now given by $g_i=\delta(t)\delta_{Np,i}$, where N_p is the number of photoexcited QD excitons per laser pulse. The multiexciton radiatively decays into a lower order multiexciton through the annihilation of one electron-hole pair, and the process continues sequentially until the QD returns to its ground state. The temporal evolution of a given multiexcitonic occupation probability can be quite straightforwardly obtained by the analytic solution of EQ. (8) which yields:

$$n_i(t) = \sum_{k=i}^{N_p} \frac{\tau_k^{(N_p-i-1)}\tau_i}{\prod_{j=i,j\neq k}^{N_p}(\tau_k - \tau_j)} e^{-\frac{t}{\tau_k}}, \qquad 0<i\le N_p \tag{10}$$

For calculating the PL intensity as a function of time we use now the calculated optical transitions from each exciton multiplex. The calculated time resolved PL spectra after a pulse with $N_p = 10$ are described in Fig. 5 where the emission intensity is displayed on a logarithmic scale. From inspecting Fig. 5 we conclude that, at relatively long times after the excitation pulse, the PL decay time of the spectral line associated with the recombination of the single exciton, is indeed τ_1. The decay times of all the other spectral lines are considerably (a factor of 4-5) shorter. It is obvious from EQ. 10 that measurements of the PL decay times of these lines do not directly yield the lifetime of any particular exciton multiplex.

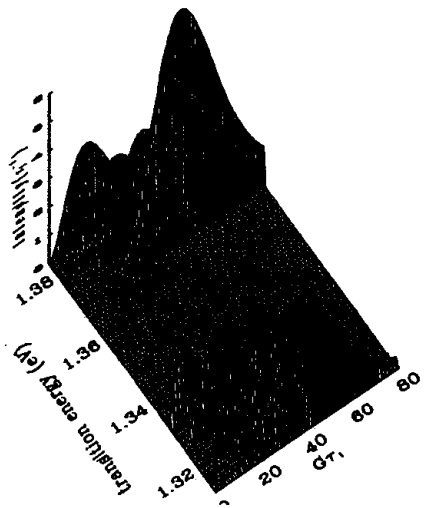

Fig 4: Calculated optical transition strengths as function of the transition energy and the cw generation rate.

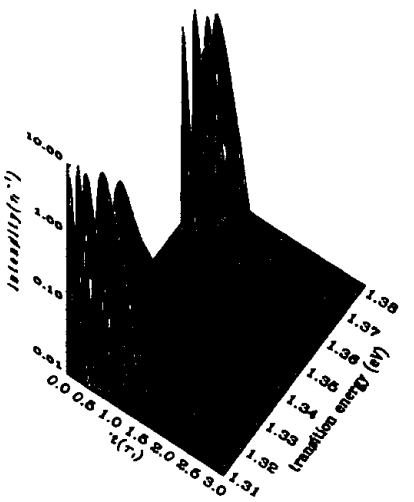

Fig 5: Calculated optical transition strengths as function of the transition energy and the time after pulse excitation of N_p=10.

For comparison with experiments in which the PL is cw measured, we temporally integrate EQ. 10 yielding this way the probability R_i that the i^{th}-multiexciton will radiatively recombine after the pulsed excitation. As expected, this yields unity for all the multiexciton orders which are smaller than or equal to N_p. Thus, for obtaining the measured cw spectrum, we simply sum over all the allowed optical transitions of these multiexcitons.

EXPERIMENTAL RESULTS

The SAQD sample studied here was fabricated by deposition of a coherently strained epitaxial layer of InAs on an AlGaAs layer deposited on a GaAs substrate using conventional molecular beam epitaxy. The SAQDs thus formed were embedded within an $Al_{0.3}Ga_{0.7}As/Al_{0.1}Ga_{0.9}As$ resonant tunneling diode-like structure [17] in order to shift the

photoluminescence (PL) emission energy above the silicon bandgap. This enabled the use of a sensitive liquid nitrogen cooled charge coupled device (CCD) array detector to perform the required very low light level spectroscopy. Furthermore, since the $Al_{0.3}Ga_{0.7}As$ barriers prevented vertical diffusion of photogenerated carriers into the SAQDs, only photons which were absorbed within the quantum wells generated carriers, which diffused laterally into the SAQDs. This allowed quite accurate estimation of the SAQD photogenerated carrier occupation. During the growth of the strained layer, the sample was not rotated. Thus a gradient in the QDs density was formed across its surface. In particular, low density areas, in which the average distance between neighboring QDs is larger than our spatial resolution could easily be found on the sample surface.

We use diffraction limited low temperature confocal optical microscope for the photoluminescence (PL) studies of the single SAQDs. A X100 in-situ microscope objective was used to focus the tunable Ti:Sapphire laser light at normal incidence on the sample. Both cw and picosecond pulsed excitations were used. The emitted light was collected by the same microscope-objective, which was accurately manipulated in three directions using computer-controlled motors. A CCD camera based active feedback loop is used for stabilizing the objective-sample working distance. The collected light was spatially filtered, dispersed by a 0.22m monochromator and detected by a nitrogen cooled CCD array detector. The system provides diffraction limited spatial resolution, both in the excitation and the detection channels. The combined spatial resolution of our system was determined by creating selective PL images of a cleaved edge of a single quantum well [19]. The spatial full width at half maximum of the SQW PL emission intensity was found to be 0.5-0.6 μm, in agreement with the expected diffraction limited optical resolution at this wavelength (~750 nm). The collection efficiency of our system was obtained from the measured spectrum of the reflected laser beam. We found that approximately 3×10^5 photons give rise to 1 CCD camera count.

The dots position and characteristic emission wavelengths are found by taking PL line scans and selective wavelength images of the SAQD sample surface [17]. We noted in such scans that at various positions on the surface spectrally sharp PL lines are observed. These lines are due to recombination of excitons within single SAQDs, as indicated by their spatial and spectral widths, which are both resolution limited [14,20]. We also note that the average distance between these SAQDs is larger than our spatial resolution. In the low power scans, (1-4 μW) the PL spectrum from each SAQD is mainly composed of a single spectral line. In contrast, however, in higher power scans, all the PL spectra contain a few PL lines, which appear mainly in pairs.

The average distance between neighboring SAQDs was comparable and larger than our spatial resolution. The PL spectra of these SAQDs show several characteristic features. In particular, the sharp spectral lines appear in one or more groups, and each such group typically contains a pair of particularly strong lines. In general, the number of groups and their PL intensity strongly depends on the power of excitation.

We note here, that since the average distance between dots is larger than our spatial resolution and is comparable to the diffusion length, the estimation of the density of the photogenerated carriers within the SAQD can be quite reliably made. In addition, the resonant-tunneling structure of our sample prohibits vertical diffusion of carriers, which were generated outside the $Al_{0.1}Ga_{0.9}As$ layer into the SAQDs. From the measured power of the excitation beam and the known index of refraction and absorption of the layers we estimated the carrier generation rate within the SAQD.

In Figs. 6 and 7 we present PL spectra from a single SAQD for various excitation powers. From the spectra, which are vertically displayed for clarity, a constant background due to PL from the bulk GaAs was subtracted. A short horizontal line represents the zero for each spectrum. Fig. 6 was obtained using cw excitation, while Fig. 7 was obtained under picosecond pulsed

excitation. The PL spectra of both cw and pulsed excitation, which were obtained from two different SAQDs, are composed of two groups of emission lines, with a few characteristic spectral lines in each group. We assigned a number to the main lines according to their spectral position. Thus, the lower energy group is composed of lines number 1 and 2 and the higher energy group is composed of lines number 4 and 5, respectively. Line number 3 is approximately positioned in-between the two groups. The energy difference between the groups amounts to 52 meV, while the difference between the pair of lines in each group is approximately 7 meV. These energies are typical for the SAQDs PL spectra. Under 1 μW cw excitation (Fig. 6) only the lowest energy PL line no. 1 is observed. As the power increases more spectral lines are observed. At 100 μW cw excitation, 5 main spectral lines are observed. When the excitation power is further increased, two broad spectral bands appear to the lower energy side of each group of discrete lines. C1 and C2 denote these bands, which dominate the PL spectrum for yet higher excitation power.

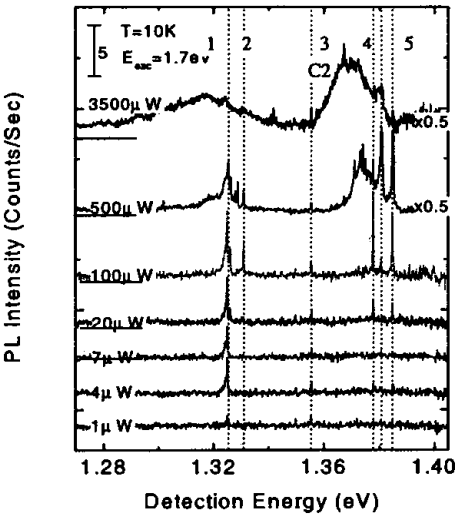

Fig 6: Single SAQD PL spectra at various CW excitation powers. The spectra are vertically shifted for clarity. The horizontal line to the left of each spectrum marks the corresponding zero-emission.

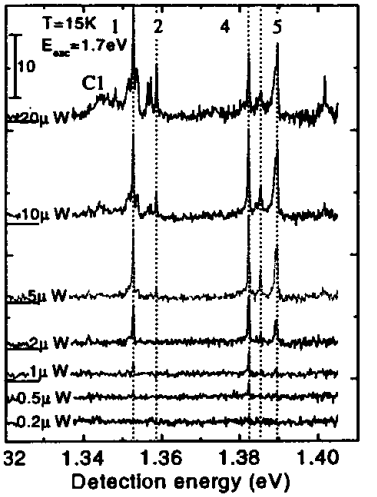

Fig 7: Single SAQD PL spectrum at various pulse excitation powers. The curves are vertically shifted for clarity.

There are two main differences between the cw and pulsed excitation as can be seen by comparing Figs. 6 and 7. First, the total PL intensity under pulse excitation is roughly an order of magnitude lower than that under cw excitation. Second, under pulsed excitation, already at very low excitation power, most of the spectral lines appear.

DISCUSSION

Our experimental findings are analyzed in terms of the theoretical model that we presented above. The advantage of this simplistic description of the QD is that its single carrier energy

levels and wavefunctions can be expressed analytically (Eq. 7). Since the model does not describe the SAQD correctly, we varied its dimensions in order to obtain maximum agreement with the measured data. Thus, by varying the base dimensions of the box, we mainly affect the energy difference between the single carrier confined levels within the box. We found out that a base dimension of ~30 nm gives rise to ~50meV energy separation between the e^1h^1 single exciton level and the e^2h^2 level. This separation is related to the energy separation between the two main groups of emission lines, which appear in the PL spectra of the SAQD. By varying now the third dimension of the box, we mainly affect the Coulomb integrals as given by Eq. (6). The values that we used were obtained with box height of 5 nm, which best fitted the characteristic 7 meV splitting between the lines in each group. Finally, we have adjusted the (small) amount by which the geometrical degeneracy is removed [21] by choosing a rectangle base with nearly equal sides. A rectangle side difference of approximately 1 nm, which resulted in 3 meV energy separation between the e^2h^2 and e^3h^3 single carrier states, best accounted for the excitation power dependence of the PL intensity of lines no. 4, and 5, and the line in between them (see Fig. 6). Note that the dimensions that we obtain are very well compared with the reported values [6].

We proceed by using our steady state rate equations (Eqs. (8)-(10)) to calculate the emitted PL spectrum as a function of the optical excitation power applied to the dot. We found that at moderate and high excitation powers, our model nicely reproduces the measured spectra and their power dependence. At low powers, however, the calculations could only resemble the measured spectra if a non-radiative recombination process is considered. Thus, a fast non-radiative decay channel is assumed for the lowest two exciton-multiplexes. This way $1/\tau_{1(2)} = 1/\tau_{1R(2R)} + 1/\tau_{NR}$ where $\tau_{1R(2R)}$ is the radiative lifetime of the exciton (biexciton) ground level and τ_{NR} is their non-radiative lifetime. We believe that for higher order multiplexes τ_{NR} can be ignored first, due to saturation and possible screening of this channel, and second due to their shorter lifetimes. By adjusting the ratio of $\tau_{1R}/\tau_{NR} \approx 0.01$ we successfully obtain the low power excitation spectra and their power dependence. The reason for this low radiative efficiency is probably due to the presence of Aluminum atoms within the dots layer and excitation transfer to neighboring dots.

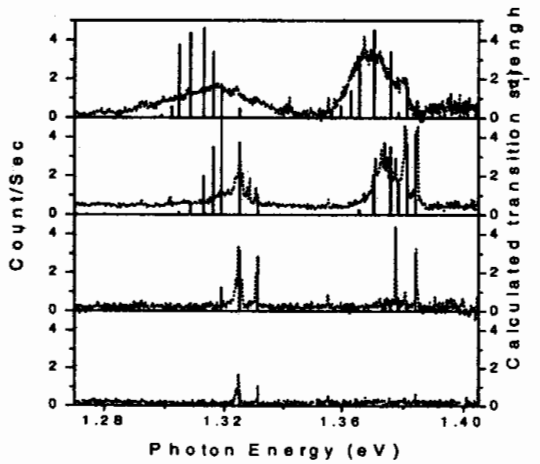

Fig 8: Comparison between the measured and calculated PL spectra for various cw excitation densities.

The results of our calculations are compared in Fig. 8 with the measured PL spectra. The main difference between the calculated and measured PL spectra is that the last one loses its discrete nature at high excitation power. This is due to the finite number (~2 - 5) of confined electron levels within the "real" SAQDs unlike that in our QD model. Thus, while in our model, the exchange energies continue to vary in a discrete manner with the multiexciton order (Fig 3), in the SAQDs it becomes continuous.

In Fig. 9 we compare the calculated and measured PL intensity of the 5 spectral lines as a function of the photogeneration power. Fig. 9a represents the cw excitation case, while Fig. 9b represents the pulsed excitation case.

We note here that in the calculations of Fig. 9b we accounted for the statistical nature of the photoexcitation process. Thus, the probability to photogenerate N_p excitons in the QD is given by,

$$P(N_p) = \frac{\exp\left(-\frac{2(N_p - G_p)^2}{G_p}\right)}{\sum_{j\geq 0}\exp\left(-\frac{2(j - G_p)^2}{G_p}\right)}, \quad N_p = 0,1,2... \tag{18}$$

where G_p is the average number of photogenerated QD excitons per laser pulse.

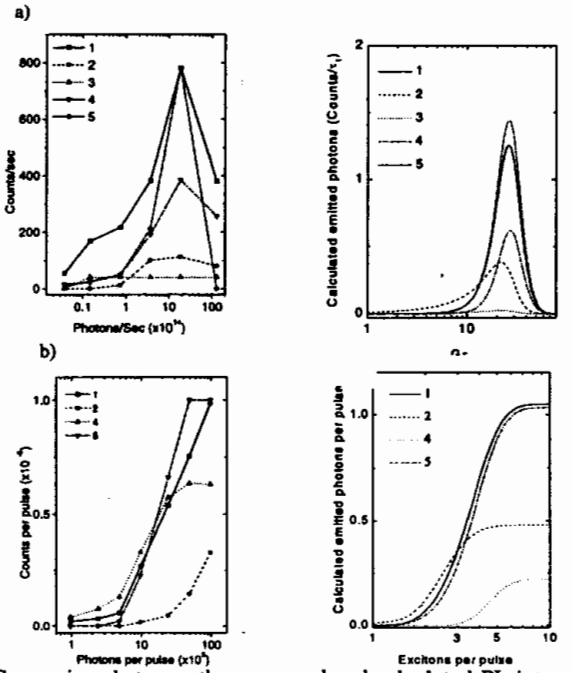

Fig 9a (9b): Comparison between the measured and calculated PL intensity of few spectral lines as function of the cw (pulse) excitation power intensity. The line numbers are in accordance with the peak numbers in Fig. 6 (Fig 7).

There is an overall agreement between the measurements and calculations as can be seen in Fig. 9. We note that our model reproduces the evolution of the PL emission with excitation power for both the CW and pulsed cases. Moreover, the absolute emission rates that we measure at the PL emission maxima are comparable with our model calculations and the efficiency of our experimental setup. The excitation efficiency at the onset of the emission detection is also comparable with our estimation and the mentioned non-radiative rates. Comparison between the abscissas of the measured and calculated curves, however, suggests that the number of excitons in the QD is proportional to the square root of the excitation power. We believe that this is the case since the assumption of 100% diffusion efficiency of photogenerated carriers into the SAQD is no longer justified at high excitation densities. It is obvious that, at these densities, lateral diffusion of carriers as well as stimulated emission, must be correctly taken into account. These processes, are beyond the scope of this work.

From the comparison between the cw and pulsed excitation, and the repetition rate the single exciton radiative lifetime (τ_{1R}) is estimated to be 3-5 ns. This lifetime completely determines now the effective decay times of the various PL lines as given by EQ. 10 and presented in Fig. 5 (note that except for the PL line which is associated with the decay of the single exciton, they are independent of τ_{NR}). We get decay times of 200-700 ps, in agreement with published data obtained by measuring the PL decay time of the SAQD's inhomogeneously broadened spectral line [22,23].

ACKNOWLEDGMENTS

The research was supported by the US-Israel Binational Science Foundation (453/97) and the Technion V. P. R fund for the promotion of research.

REFERENCES

1. D. Bimberg, M. Grundmann and N.N. Ledentsov, Quantum Dot Heterostructures, (John Wiley & Sons, UK, 1998).
2. I. N. Stranski and L. Krastanow, Akad. Wiss. Lit. Math.-Natur Kl. 11b **146**, 767 (1939).
3. J. Y. Marzin, J. M. Gerard, A. Israel et al, Phys. Rev. Lett. **73**, 716 (1994).
4. H. Drexler, D. Leonard, W. Hansen, Phys. Rev. Lett. **73**, 2252 (1994).
5. D. Leonard, P. M. Petroff et al., Phys. Rev. B **50**, 8086 (1994).
6. D. Leonard, K. Pond, P. M. Petroff, Phys. Rev. B **50**, 11687 (1994).
7. M. Bayer, T. Gutbrod, A. Forchel et al, Phys. Rev. B **58**, 4740 (1998).
8. M. Ikezawa, Y. Masumoto, T. Takagahara and S.V. Nair, Phys. Rev. Lett **79**, 3522 (1997).
9. L. Landin, M. S. Miller, M. E. Pistol, C. E. Pryor, L. Samuelson, Science **280**, 262 (1998).
10. R. Heitz, A. Kalburge, Q. Xie, M. Grundmann et al, Phys. Rev. B **57**, 9050 (1998).
11. K. Brunner, G. Abstreiter, G. Bohm et al, Phys. Rev. Lett. **73**, 1138 (1994).
12. H. Kamada, H. Ando, J. Temmyo, and T. Tamamura, Phys. Rev. B **58**, 16243 (1998).
13. Y. Toda, S. Shinomori, K. Suzuki and Y. Arakawa, Phys. Rev. B **58**, 10147 (1998).
14. D. Gammon, E. S. Snow, B. V. Shanabrook et al, Phys. Rev. Lett. **76**, 3005 (1996).
15. A. Franceschetti, L. W. Wang, H. Fu and A. Zunger, Phys. Rev. B **58**, R13367 (1998).
16. A. Barenco and M. A. Dupertuis, Phys. Rev. B **52**, 2766 (1995).
17. E. Dekel, D. Gershoni, E. Ehrenfreund et al, Phys. Rev. Lett. **80**, 4991 (1998).
18. S. Adachi, J. Appl. Phys. **58**, R1 (1985).
19. T. D. Harris, D. Gershoni, R. D. Grober et al, Appl. Phys. Lett. **68**, 988 (1996).
20. H.F. Hess, E. Betzig, T. D. Harris, L. N. Pfeiffer and K. W. West, Science **264**, 1740 (1994).
21. J. Kim, L. W. Wang and A. Zunger, Phys. Rev. B **57**, R9408 (1998).
22. S. Grosse, J. H. H. Sandmann, G. von Plessen et al, Phys. Rev. B **55**, 4477 (1997).
23. M. Bresken, M. Lindberg, M. Sopanen et al, Phys. Rev. B **58**, 15993 (1998).